International Journal of Current Research and Modern Education (IJCRME)
ISSN (Online): 2455 – 5428 & Impact Factor: 3.165
Special Issue, NCFTCCPS - 2016

IMPLEMENTATION OF THIRD HARMONICS INJECTION BY MATRIX CONVERTER

P. Prakash*, M. Sathishkumar & G. Sathishkumar*****
Department of Electrical and Electronics Engineering, Gnanamani College of Technology, Tamilnadu

Abstract:

Due to the merits of sinusoidal input currents and excellent conversion efficiency, buck-type active third-harmonic injection converters have received increasing attention in recent years. However, three major problems of these converters still exist in theory and practice. First, the existence of the dc-link capacitor, utilized by early researchers, causes inrush transient and distorts the input currents. Second, in some specific situations, such as wind energy conversion system and flexible ac transmission system, these converters' capabilities of generating input reactive power need sufficient improvements. Third, proper selection of the third-harmonic injection inductor is the key challenge to implement these converters, since the inductor affects not only the current ripple but also the tracking performance of the third-harmonic current. To solve these problems, this paper studies the two-stage matrix converter with third harmonics injection and demonstrates that the dc-link capacitor can be removed by bidirectional implementation and proper control of the rectifier. Then, an algorithm enhancing the input reactive power capability is developed. Thus, sinusoidal input currents are achieved and the reactive power control range is extended significantly. Moreover, the design criteria of the third-harmonic injection inductor are discussed. Finally, the proposed method is verified by simulation and experimental results.

Index Terms: AC–AC Power Conversion, Indirect Matrix Converter (IMC), Narrow Pulse Width, Reactive Power, Third-Harmonic Injection & Voltage Transfer Ratio

1. Introduction:

UE to the attractive characteristics such as low cost, simple D and reliable structure, high efficiency, and low electromagnetic interference noise, three-phase diode rectifier front-end converters have been widely applied to ac–ac power conversion applications such as adjustable speed ac drives (ASDs) and uninterrupted power supplies. However, one of the undesirable features of the diode rectifier front-end converters is the greatly distorted line current, which may cause harmonic pollution in the power system [1]. Usually, there are two solutions to solve this problem: one is using the "green" active power factor correction (PFC) converters to replace the diode rectifier front-end converters [2]; the other is applying the active power filter technique to compensate for the harmonic current generated by the diode rectifiers.

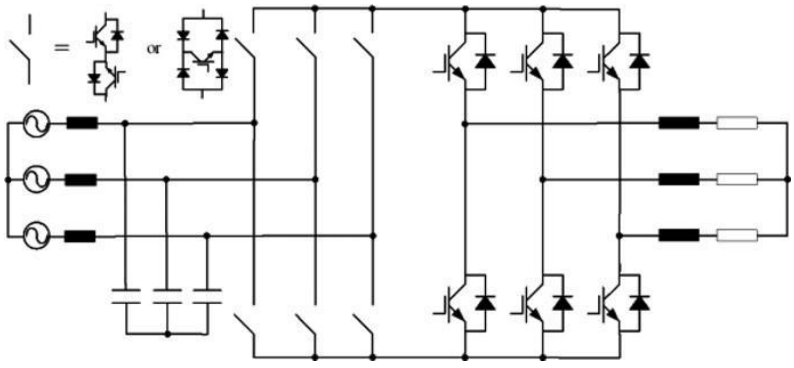

Figure 1: Conventional IMC topology

For the first solution, voltage-source-type back-to-back pulse width modulation (PWM) converters (V-BBC) and current-source-type back-to-back PWM converters (C-BBC) are two typical active PFC converters. Both of them carry advantageous features such as bidirectional power flow, sinusoidal input cur-rents and controllable input power factor. However, the heavy and bulky energy storage elements in the dc-link hinder the compactness design and system integration of converters [3]–[5]. An alternative is the matrix converters (MCs), which have attracted an increasing attention in recent years due to the absence of energy storage elements [6]–[11]. MCs can be classified into two types: direct matrix converter (DMC) and indirect matrix converter (IMC). The IMC topology illustrated in Fig. 1 pro-vides zero-current commutation that is not available in DMC. Besides, the clamp circuit for overvoltage protection is simpler compared to DMC. Due to the features above, IMC has been extensively investigated recently [8]–[11]. In most applications, a unity input power factor operating condition is preferred for MCs. However, when MCs are applied in a wind energy conversion system (WECS) [12] or a flexible ac transmission system [13], there is a requirement of generating input reactive power. For IMCs employing the conventional modulation [11], the in-put reactive power can be regulated to some extent by changing the input displacement angle. Unfortunately, the maximum volt-age transfer ratio achievable decreases with the decreasing of the input power factor [14], [15], which is of great disadvantage in ASD applications since the output capability is restricted. More-over, strict synchronization in modulation between the rectifier and the inverter is necessary for IMCs. That is, the inversion stage must experience a synthesis of the output space vector in every sub switching cycle of the rectification stage. Thus, the input and output performance may be degraded due to the non-linearity caused by narrow pulse width [16].

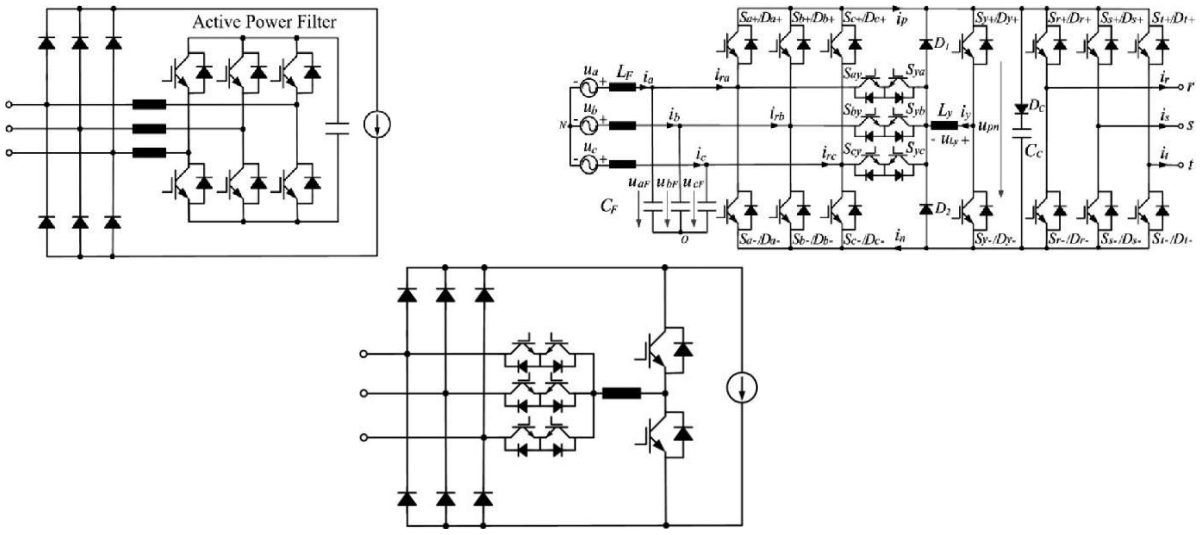

Figure 2 & 3: Buck-type active third-harmonic injection converter.

Regarding the second solution, two schemes have been pro-posed and researched. One is to install an extra three-phase active power filter in parallel to the diode rectifier front-end converter [17], [18], as shown in Fig. 2. The other is to employ the active third-harmonic injection technique to improve the input current quality [19]–[27], as presented in Fig. 3. The active third-harmonic injection concept is first introduced in [19], where a three phase grid-connected photovoltaic inverter with-out electrolytic capacitors for improved lifespan is proposed. In [20], this circuit is applied to the conventional diode rectifier-fed inverter which has a small dc-link capacitor for

the purpose of reducing the input current harmonics. Although the quality of the input current is improved greatly, the overvoltage problem may occur when feeding low output power factor loads or in regenerative operation mode due to the lack of energy storage components in the dc-link and the inherent characteristic of unidirectional power flow. In [27], the design and implementation of the unidirectional active third-harmonic injection circuit, feeding a buck converter for dc distribution systems, are presented, and the derivation of the bidirectional ac–ac converter, based on active third-harmonic injection circuit, is also investigated. However, as in the situation of [20], a film capacitor is placed in the dc-link to provide the required cur-rent path. In theory, it causes inrush transient in the dc-link capacitor and input capacitors, and distorts the input currents, especially when the capacitance of the dc-link capacitor and the input capacitor are comparable. Besides, so far the detailed studies of the bidirectional third-harmonic injection-based ac– ac converter has not been reported in the literature, including the input reactive power control range, voltage transfer ratio, and experimental verifications of the full functionality of the topology.

In this paper, the functionality and performance of the third-harmonic injection two-stage matrix converter (3TSMC) are investigated systematically. It is demonstrated that the dc-link capacitor could be removed through bidirectional implementation and proper control of the rectifier. Besides, the operating principles of 3TSMC are analyzed in detail. An algorithm for achieving sinusoidal input currents and significantly extending the input reactive power control range without lowering the voltage transfer ratio is developed, and mathematical proof of the correctness of the algorithm is also provided. Based on the analysis of the operating principles, a detailed comparison between IMCs and 3TSMC is presented. Moreover, modulation strategies of 3TSMC are discussed, and the narrow pulse is-sue is analyzed and compared with that of IMCs. In addition, the system design is carried out, and the design criteria of the third-harmonic injection inductor, considering both the current ripple and the third-harmonic current tracking performance, are introduced. Finally, the proposed method and all the theoretical analyses are verified by simulation and experimental studies.

This paper is organized as follows: Section II introduces the topology and operating principles of 3TSMC, presents the solution to cancel the dc-link capacitor, and discusses the algorithm that can achieve sinusoidal input currents and extend the input reactive power significantly; Section III presents the modulation strategies in detail, along with the discussion of narrow pulse width issue; Section IV introduces the system design including the design criteria of the third-harmonic injection inductor, followed by the power loss analysis and efficiency evaluation; Section V shows the simulation and experimental results to verify the presented method; Section VI draws the final conclusion of this paper.

2. Topology and Operating Principles:

A. Topology:

The topology of 3TSMC is shown in Fig. 4. The main circuit consists of an input *LC* filter, a bidirectional rectifier, a clamp circuit consisting of a fast recovery diode *Dc* and a film capacitor *Cc*, an active third-harmonic current injection circuit and a conventional VSI. The active third-harmonic current injection circuit is composed of three bidirectional switches, a third-harmonic injection inductor and a bridge leg. Under nor-mal operation conditions, only one of the three bidirectional switches is turned on to inject the third-harmonic current into the corresponding input phase. According to the requirements of the load, the VSI provides three-phase output voltages with variable frequency and amplitude. The clamp circuit is used to absorb the energy stored

in the leakage inductance of the load when the system shutdown. Regarding the topologies presented in [20] and [27], a dc-link capacitor is needed to provide the required current path of the third-harmonic injection inductor. Nevertheless, it causes inrush transient and distorts the input currents. Thus, these topologies are not well structured and the proof of sinusoidal input currents in [27] is not applicable. Actually, through bidirectional implementation and proper control of the rectifier, the dc-link capacitor can be eliminated. In this paper, commutation of the rectifier is controlled to occur at the moment of zero dc-link current. For example, commutation between the upper switches S_{a+}, S_{b+} and S_{c+} is arranged when the current i_p is equal to zero. Thus, the dc-link capacitor is removed and the switching losses of the rectifier can also be ignored. Besides, the clamp circuit can also provide the required current path for sector transition.

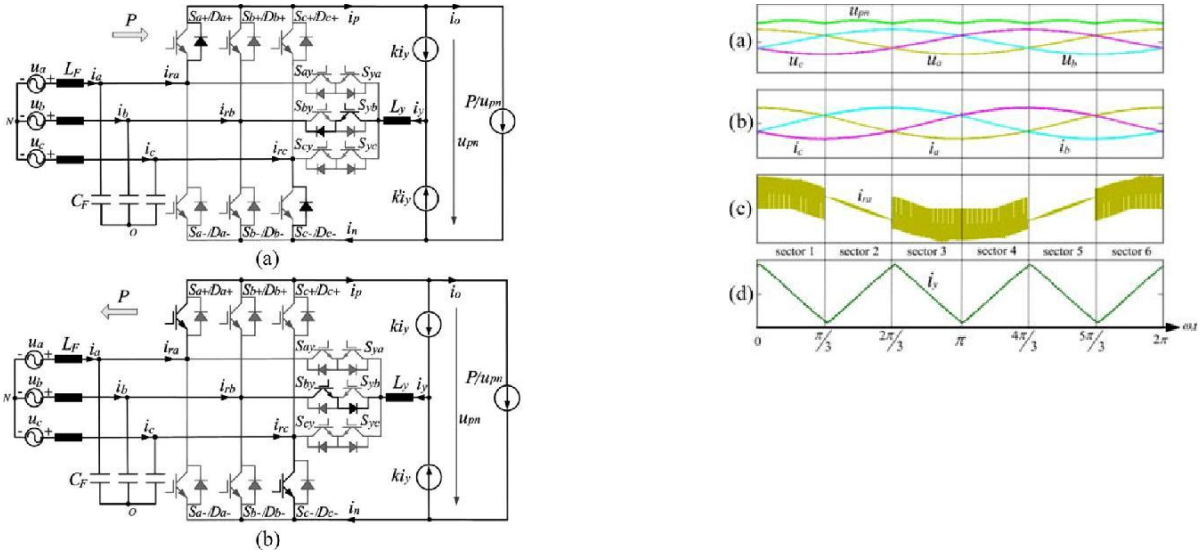

Figure 4 & 5: Equivalent circuit diagram of 3TSMC (assuming $u_a > u_b > u_c$ and $u_b < 0$). (a) Forward power flow. (b) Reverse power flow.

Compared with conventional IMCs, although two more switches are added and an extra third-harmonic injection inductor is introduced, the amplitude of the current imposed on the third-harmonic injection inductor is relatively low and the input current quality of the rectifier is improved due to the existence of the third-harmonic injection inductor. Besides, the switches of the rectifier commutate at the line frequency. Thus, low cost switches with low switching speeds are applicable. This helps to reduce the system cost especially for high power converter applications.

B. Operating Principles:

The operating principles of 3TSMC are described as follows: For the switches S_{a+}, S_{b+} and S_{c+} of the rectifier, the switch connected to the input phase with the highest voltage is kept on; for the switches S_{a-}, S_{b-} and S_{c-}, the switch connected to the input phase with the lowest voltage is kept on. The switches S_{y+} and S_{y-} in third-harmonic current injection circuit are controlled to form the third-harmonic current i_y flowing through the inductor L_y. The bidirectional switch connected to the input phase with the lowest absolute voltage is kept on to inject the third-harmonic current. For example, when the input voltages satisfy $u_a > u_b > u_c$ (denoted as sector 1), switches S_{a+} and S_{c-} in the rectifier and the bidirectional switches S_{yb} and S_{by} in the third-harmonic current injection circuit are turned on, as shown in Fig. 5, and so forth. In this manner, sinusoidal three-phase input currents and controllable input power factor are attainable. The key waveforms of the rectifier and third-harmonic current injection

circuit are shown in figure.

C. PFC Algorithm and its Mathematical Proof:

Assume the converter has no power loss and the output power is constant, an algorithm for achieving sinusoidal input currents and controllable input power factor is developed, along with the mathematical proof of the correctness of the algorithm.

Three-phase symmetrical input voltages can be expressed as

$$u_a = U\cos(\omega_i t)$$
$$u_c = U\cos(\omega_i t + 2\pi/3)$$

Where U and ω_i are the amplitude and angular frequency of the input voltages, respectively. Sort the input voltages according to the relationships of the instantaneous values as follows:

$$u_{max} = \max(u_a, u_b, u_c)$$
$$u_{mid} = \mathrm{mid}(u_a, u_b, u_c) \qquad (2)$$
$$u_{min} = \min(u_a, u_b, u_c)$$

Where u_{max}, u_{mid} and u_{min} represent the maximum value, medium value, and minimum value among the three-phase input voltages; max, mid, and min are the operators of the maximum value, medium value and minimum value, respectively.

For the remaining sectors, similar results can be obtained, and the derivation process will not be repeated here. Thus, three-phase sinusoidal input currents and controllable input power factor are achieved via the algorithm above. It should be noted that, in the aforementioned derivation process, the control method is applicable to both directions of the power flow. Positive P indicates forward power flow and the contrary is the case when P is negative.

In sector 1, from the switching states, it is found that the current i_{rb} is equal to the opposite value of the third-harmonic injection current i_y. Suppose the input currents are sinusoidal and the input power factor is controllable, then the average value of i_{rb} can be obtained as

$$\begin{aligned} i_{rb} &= -i_y = I_{pm}\cos(\omega_i t - 2\pi/3) + I_{qm}\sin(\omega_i t - 2\pi/3) \\ &= GU\cos(\omega_i t - 2\pi/3) + I_{qm}\sin(\omega_i t - 2\pi/3) \\ &= GU\cos(\omega_i t - 2\pi/3 + \phi)\cos\phi \end{aligned}$$

D. Comparisons between IMCs and 3TSMC:

The differences in topology and operating principles between IMCs and 3TSMC would result in some different external characteristics, such as the input reactive power control range, the voltage transfer characteristic, as well as requirements of the input filter. It can be seen from the mathematical proof of the PFC algorithm that the input displacement angle range in 3TSMC is quite different from that of conventional IMCs (assume conventional modulation is used in IMCs), since the input displacement angle range in IMCs is only from $-\pi/3$ to $\pi/3$. Consequently, the reactive power control range at the input side of IMCs and 3TSMC can therefore be calculated as shown in (10) and (11), respectively. 3TSMC and conventional IMCs are shown in Fig. 7. As shown from the spectrums, the dominant harmonic current is around the second-order switching frequency in 3TSMC and about the first-order switching frequency in IMCs. Besides, the magnitudes of the dominant harmonic current in 3TSMC are less than that of IMCs. The total harmonic distortion (THD) of the current i_{ra} in 3TSMC and IMCs are 57% and 153%, respectively. Thus, a higher corner frequency of the input filter can be selected and a lower attenuation of the dominant harmonic current is required in 3TSMC [28], which imply a smaller size of the input filter. The detailed comparisons between IMCs

and 3TSMC are shown in Table I.

3. Modulation Strategies:

A. Modulation of the Rectifier and the Third-Harmonic Current Injection Circuit:

As described before, the switches in the rectifier and the bidirectional switches in the third-harmonic current injection circuit operate at a low frequency, and the states of the switches are determined only by the input voltages. Table II shows the modulation of the rectifier and the third-harmonic current injection circuit in one line cycle. The switch states of the bridge leg in the third-harmonic current injection circuit are complementary, and the steady-state duty ratio of switch S_{y+} is k. For the third-harmonic current injection circuit, to prevent short circuit of the input side and open circuit of the inductor L_y , only one of the three bidirectional switches is kept on at any time, thus a proper commutation strategy should be developed to guarantee the safe operation of the converter. Similar to that of DMC, the current-based four-step commutation strategy is utilized in this project [7].

B. Modulation Strategy of the Inverter:

As shown in Fig. 6, the six-pulse shape dc-link voltage of 3TSMC is quite different from the high frequency PWM dc-link voltage in conventional IMCs [11]. Therefore, the modulation strategy of the inverter is different from that of conventional IMCs. For the inversion stage of 3TSMC, the carrier modulation is employed and the concrete analysis is given as follows: Assume the symmetrical three-phase output reference volt-ages are the angular frequency and initial phase of the expected output voltages, respectively. To improve the utilization of the dc-link voltage, a zero sequence voltage u_{no} is added to the phase leg reference voltages without impacting the output fundamental line-line voltages. Then the phase leg reference voltages, known as the modulation signals, are modified as follows: The modified modulation signal

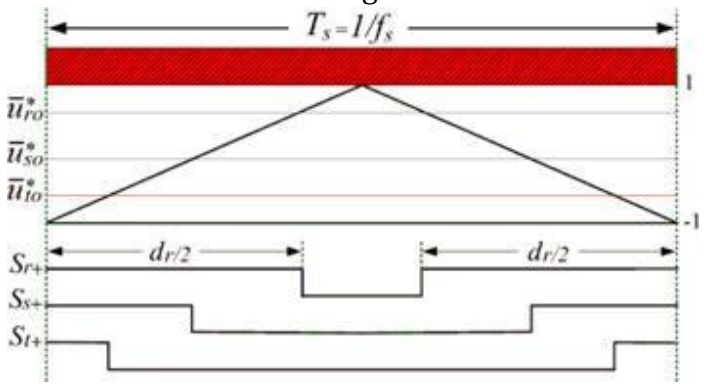

Figure 8: Modulation diagram of the inverter of 3TSMC

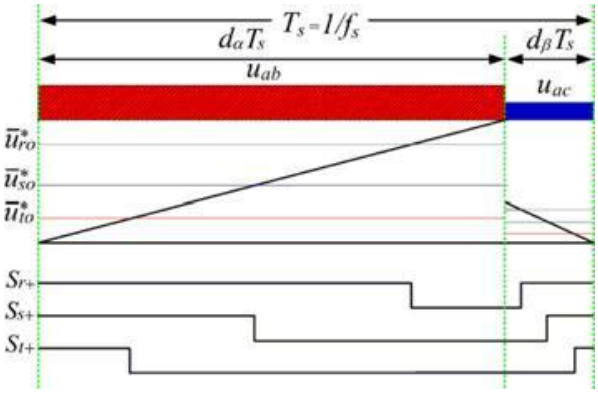

Figure 9: Modulation diagram of the inverter of conventional IMCs

The quasi-third harmonic zero sequence voltage is selected identically as that used in [29] and can be expressed as according to the fundamental principles of the carrier modulation, the phase leg modulation signals should be normalized referring to the dc-link voltage u_{pn} before the calculation the phase leg duty ratios. It should be noted that the maximum out-put voltage of a phase leg (refers to the virtual middle point of the dc-link) is half of the dc-link voltage, therefore the normalized modulation signals u^{-*}_{io} are obtained as follows: Based on the carrier modulation schematic diagram illustrated in Fig. 8 and the geometry theory, the phase leg duty ratios d_i can be calculated as according to the analysis above, the modulations of the rectifier and inverter in 3TSMC are independent. Thus, synchronization between the rectifier and inverter is not required. Com-pared with conventional IMCs, realization of the modulation in 3TSMC is therefore more flexible, which has potential advantages in multiple drive systems [30]. Meanwhile, the nonlinearity caused by narrow pulse width in conventional IMCs is improved. The modulation diagram of the inverter of 3TSMC is illustrated in Fig. 8, where T_s is the switching period and f_s is the switching frequency. As a comparison, modulation diagram of the inverter of IMCs is also shown in Fig. 9 to illustrate the narrow pulse width issue, where d_α and d_β are the duty cycles of the rectification stage.

The essential reason of conventional IMCs generating narrow pulses is that the modulation of the rectifier and inverter must be synchronized strictly due to the absence of energy storage elements in the dc-link. When the desired input current vec-tor is located in the sector boundaries, one of the duty cycles in the rectification stage would be very short. As a result the modulation of the inversion stage is difficult to realize in such a short time due to the physical limits in a practical system. Also, adopting the round-up method to ignore narrow pulses causes distortions of input and output waveforms [16].

Different from that of IMCs, the six-pulse waveform dc-link voltage in 3TSMC can be considered as a constant voltage source in one switching period. Therefore, the inversion stage of 3TSMC is modulated only once in each switching period, then the narrow pulse problem is relieved.

4. System Design and Power Loss Analysis:

A. System Design:

1) Third-Harmonic Injection Inductor Design: An important issue in system design is the design of the inductor L_y , since the inductor concerns the tracking performance of third-harmonic current, as well as the quality of input current. The design criteria are as follows: 1) the ripple current of the inductor should be suppressed at a reasonable level. 2) The tracking performance of *the* third-harmonic injection current should be excellent enough. In [27], the selection of the inductor L_y is analyzed with only the ripple current being considered. However, it should be noted that an inductor of large inductance is helpful to reduce the ripple current, but it makes the current response slow, so a tradeoff should be made between these two aspects.

The current flowing through L_y consists of a quasi-third harmonic current $I_{3r\,d}$ and a ripple current i_y . The maximum value of i_y is hoped to be limited to $\gamma I_{3r\,d}$, where γ is the ripple index and $I_{3r\,d}$ is the amplitude of i_y .

According to the operating principles mentioned previously, the third-harmonic injection current i_y increases when the switch S_{y+} is turned on and decreases when the switch S_{y+} is turned off. Thus, for a given inductor the ripple current is determined by the voltage across the inductor when the switch S_{y+} is turned on and its duration. Take sector 1 ($0 \le \omega_i t \le \pi/3$) for

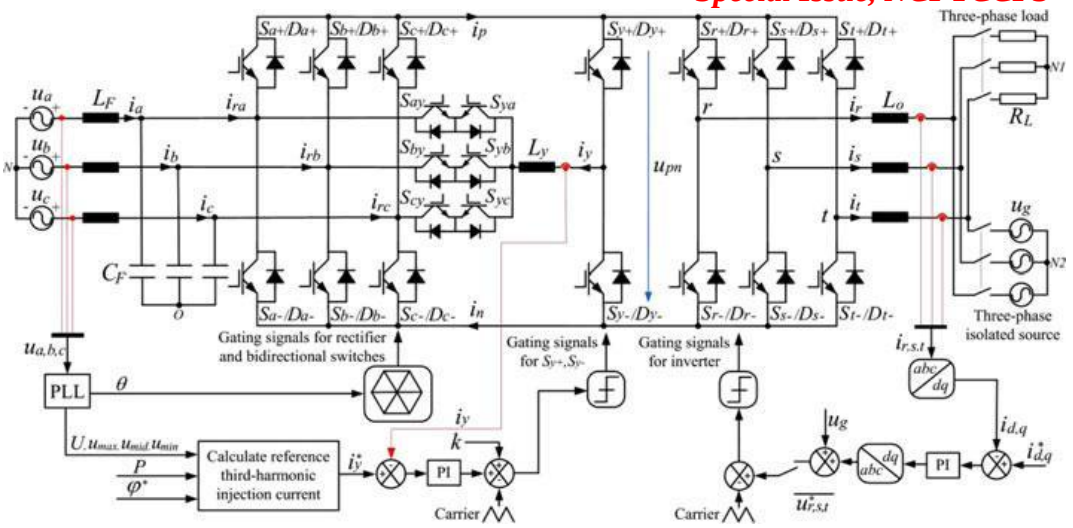

Figure 10: System control schematic diagram of 3TSMC

Component	Forward power flow ($\varphi_o \in [-\pi/2, \pi/2]$)		Reverse power flow ($\varphi_o \in [-\pi, -\pi/2) \text{and} (\pi/2, \pi]$)	
	I_{AVG} [A]	I_{RMS} [A]	I_{AVG} [A]	I_{RMS} [A]
S_{i+}, S_{i-} (i=a, b, c)	0	0	$I_m\frac{\sqrt{3}}{2\pi}$	$I_m\sqrt{\frac{1}{6}+\frac{\sqrt{3}}{8\pi}}$
D_{i+}, D_{i-} (i=a, b, c)	$I_m\frac{\sqrt{3}}{2\pi}$	$I_m\sqrt{\frac{1}{6}+\frac{\sqrt{3}}{8\pi}}$	0	0
S_{iy} , S_{yi} (i=a, b, c)	$I_m\frac{2-\sqrt{3}}{2\pi}$	$I_m\sqrt{\frac{1}{12}-\frac{\sqrt{3}}{8\pi}}$	$I_m\frac{2-\sqrt{3}}{2\pi}$	$I_m\sqrt{\frac{1}{12}-\frac{\sqrt{3}}{8\pi}}$
S_{y+}, S_{y-}	$\frac{3I_m}{4\pi}(2-\sqrt{3}\ln 3)$	$I_m\sqrt{\frac{1}{8}+\frac{3\sqrt{3}}{4\pi}\ln\frac{3}{4}}$	$\frac{3I_m}{4\pi}(2-2\sqrt{3}+\sqrt{3}\ln 3)$	$I_m\sqrt{\frac{1}{8}-\frac{3\sqrt{3}}{4\pi}\ln\frac{3}{4}-\frac{3\sqrt{3}}{8\pi}}$
D_{y+}, D_{y-}	$\frac{3I_m}{4\pi}(2-2\sqrt{3}+\sqrt{3}\ln 3)$	$I_m\sqrt{\frac{1}{8}-\frac{3\sqrt{3}}{4\pi}\ln\frac{3}{4}-\frac{3\sqrt{3}}{8\pi}}$	$\frac{3I_m}{4\pi}(2-\sqrt{3}\ln 3)$	$I_m\sqrt{\frac{1}{8}+\frac{3\sqrt{3}}{4\pi}\ln\frac{3}{4}}$
S_{i+}, S_{i-} (i=r, s, t)	$I_{om}(\frac{1}{2\pi}+\frac{3m\cos\varphi_o}{8\pi}\ln(2+\sqrt{3}))$	$I_{om}\sqrt{\frac{1}{8}+\frac{m\cos\varphi_o}{4\pi}(\frac{3\sqrt{3}}{8}\ln 2-\frac{9\sqrt{3}}{16}\ln 3-\frac{5\pi}{16})}$	$I_{om}(\frac{1}{2\pi}+\frac{3m\cos\varphi_o}{8\pi}\ln(2+\sqrt{3}))$	$I_{om}\sqrt{\frac{1}{8}+\frac{m\cos\varphi_o}{4\pi}(\frac{3\sqrt{3}}{8}\ln 2-\frac{9\sqrt{3}}{16}\ln 3-\frac{5\pi}{16})}$
D_{i+}, D_{i-} (i=r, s, t)	$I_{om}(\frac{1}{2\pi}-\frac{3m\cos\varphi_o}{8\pi}\ln(2+\sqrt{3}))$	$I_{om}\sqrt{\frac{1}{8}-\frac{m\cos\varphi_o}{4\pi}(\frac{3\sqrt{3}}{8}\ln 2-\frac{9\sqrt{3}}{16}\ln 3-\frac{5\pi}{16})}$	$I_{om}(\frac{1}{2\pi}-\frac{3m\cos\varphi_o}{8\pi}\ln(2+\sqrt{3}))$	$I_{om}\sqrt{\frac{1}{8}-\frac{m\cos\varphi_o}{4\pi}(\frac{3\sqrt{3}}{8}\ln 2-\frac{9\sqrt{3}}{16}\ln 3-\frac{5\pi}{16})}$

Table IV: Specifications of the Fabricated Devices

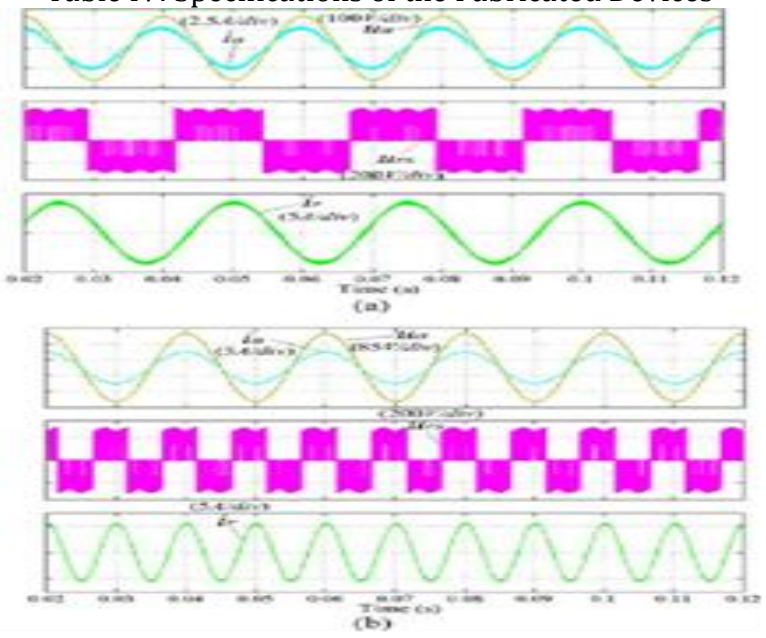

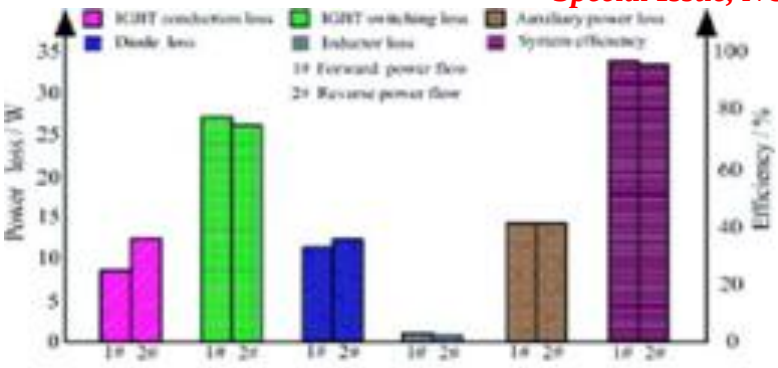

Figure 11: Calculated power loss distribution and efficiency diagram of 3TSMC.

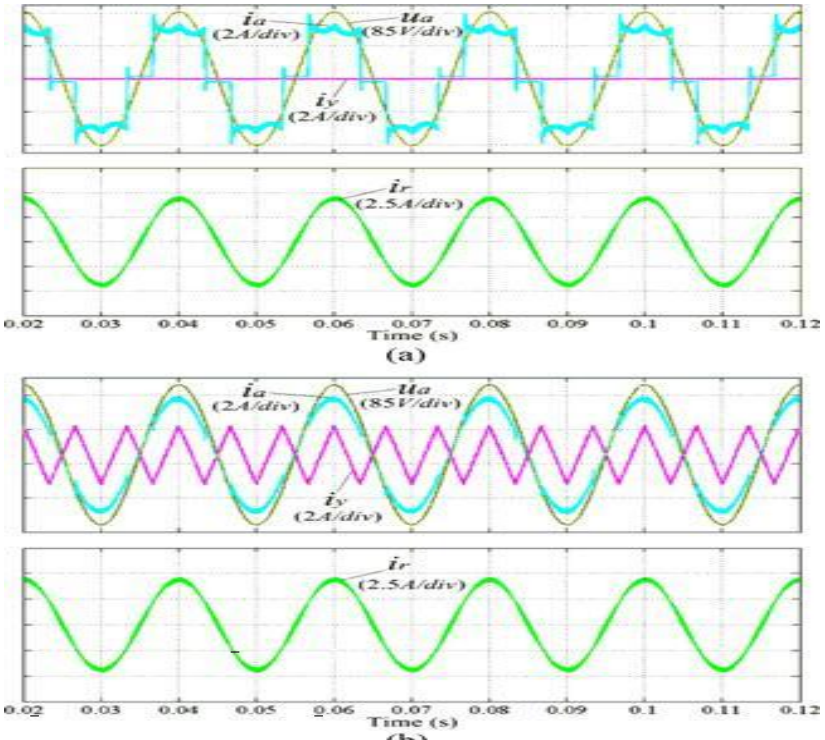

Figure 12: Simulated waveforms of 3TSMC with the third-harmonic injection circuit (a) disabled and (b) enabled.

B. Experiments:

To validate the theoretical analyses and simulated results, a laboratory prototype of 3TSMC with the specifications given in Table III is built, as shown in Fig. 17. For the rectifier switches and bidirectional switches in the third-harmonic injection circuit, the conduction losses are the major part, thus IGBT IHW30N120R2 (1200 V/30 A, Infineon) with low saturation voltage is selected. Switches on the legs of the third-harmonic injection circuit and the inverter stage are switching at high frequency, thus, combined with ultra fast recovery diode. Experimental waveforms of 3TSMC with different input power factors. (a) Displacement angle is $\pi/6$. (b) Displacement angle is $-\pi/6$. (c) Displacement angle is $\pi/2$. (d) Displacement angle is $-\pi/2$. CH1 is the input voltage u_a (85 V/div), CH2 is the input current i_a (5 A/div), CH3 is the output line-line voltage u_{rs} (250 V/div), CH4 is the output current i_r (7 A/div), time scale is 10 ms/div in (a) and (b). CH1 is the input voltage u_a (85 V/div), CH2 is the input current i_a (10 A/div), CH3 is the voltage across the inductor L_y (250 V/div), CH4 is third-harmonic injection current (10 A/div) and time scale is 10 ms/div in (c) and (d).

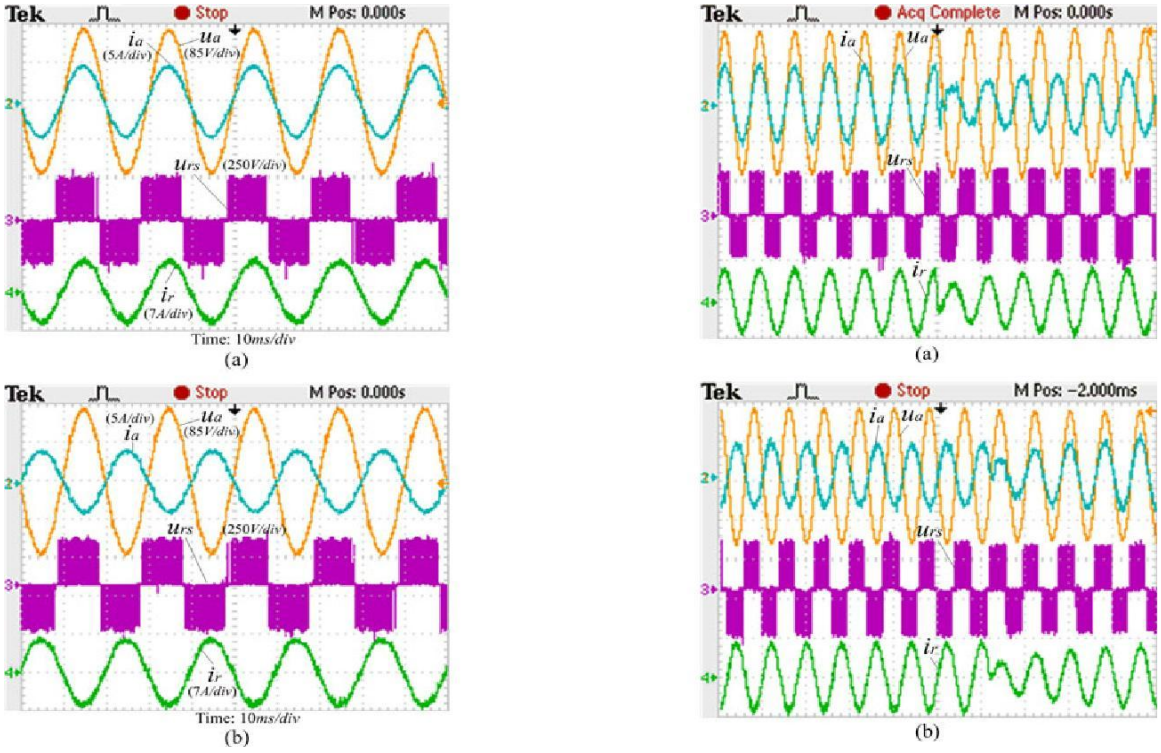

Figure: Experimental waveforms of 3TSMC when in (a) forward and (b) reverse power flow operation conditions. CH1 is the input voltage u_a , CH2 is the input current i_a , CH3 is the output line-line voltage u_{rs} , CH4 is the output current i_r .

Experimental waveforms of 3TSMC with the output active current reference stepping from (a) +6 to −6 A and (b) −6 to +6 A. CH1 is the input voltage u_a (85 V/div), CH2 is the input current i_a (5 A/div), CH3 is the output line-line voltage u_{rs} (250 V/div), CH4 is the output current i_r (7 A/div), time scale is 25 ms/div. DSEP29-12A (1200 V/30 A, IXYS), high speed IGBT IGW40N120H3 (1200 V/40 A, Infineon) is used. The control of 3TSMC is realized by a combination of DSP TMS320F28335 and FPGA EP2C8T144C8N. The experimental results shown in Figs. 18–22 correspond to the simulated results shown in Figs. 12–16, and the experimental conditions and commands are exactly the same as those in the simulations. As can be seen from Figs. 18–22, the experimental results match the simulated results very well, except for a slight reduction in the amplitudes of the input and output current when fed resistive load. The subtle difference is primarily caused by the power losses in the prototype. In Fig. 21, THD of the input current and input power factor measured by power quality analyzer FLUKE430 are 2.74% and 0.997 for motoring operation mode. When in regenerating operation mode, a THD of 3.69% and a power factor of 0.995 are achieved. Thus, the excellent characteristics of 3TSMC are verified experimentally.

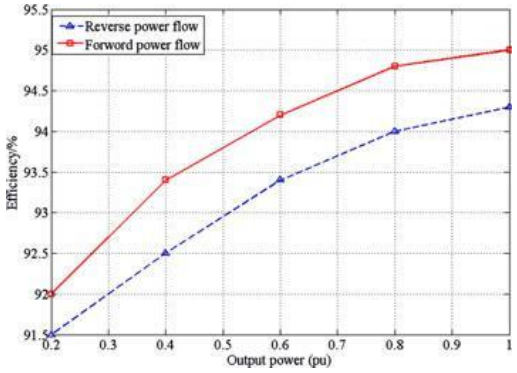

Figure: Measured efficiency of 3TSMC prototype

To verify the accuracy of the losses modeling, the system efficiency is measured by a three-phase wattmeter in the experiments as shown in Fig. 23. And the nominal efficiency measured is 95.0% in motoring operation mode and 94.3% in regenerating operation mode, which are a bit lower than the calculated ones. This can be explained by the fact that the losses dissipated on input capacitors, PCB traces and current sensors are not considered in theoretical calculation.

6. Conclusion:

In this paper, the major problems of the buck-type active third-harmonic injection converter are solved through systematical investigation of 3TSMC topology based on third-harmonic injection technique. It is demonstrated that the dc-link capacitor that causes inrush transient and distorts the input currents, can be removed through bidirectional implementation and proper control of the rectifier. A PFC algorithm is developed, which addresses the disadvantage of limited capability of generating the input reactive power in conventional IMCs. Thus, the input reactive power control range is extended significantly and the input power factor angle can vary from $-\pi/2$ to $\pi/2$, irrelevant to the output conditions. By considering both the current ripple and current tracking performance, the design criteria of the third-harmonic injection inductor are discussed, and a general guideline for designing and realizing of those converters is provided. The 3TSMC possesses the same essential features as conventional IMCs such as sinusoidal input and output currents, and bidirectional power flow. Besides, it has some superior performance such as enhanced input reactive power capability, a maximum voltage transfer ratio of 0.866 under all operation conditions, improved input currents, as well as flexible implementation of the modulation strategies. All the advantages make the 3TSMC an attractive candidate for ac drives, WECS and other applications.

7. References:

1. IEEE Recommended Practices and Requirements for Harmonic Control in Electric Power Systems, IEEE Standard 519, 1992.
2. Kuperman, U. Levy, J. Goren, A. Zafranski, and A. Savernin, “High power Li-ion battery charger for electric vehicle,” in Proc. 7th Int. Com-patibility Power Electron. Conf. Workshop, Jun. 2011, pp. 342–347.
3. P. D. Ziogas, Y. G. Kang, and V. R. Stefanavic, “Rectifier-inverter frequency changer with suppressed DC link components,” IEEE Trans. Ind. Appl., vol. IA-22, no. 6, pp. 1027–1036, Nov. 1986.
4. S. Kim, S. K. Sul, and T. A. Lipo, “AC to AC power conversion based on matrix converter topology with unidirectional switches,” in Proc. IEEE Appl. Power Electron. Conf., Feb. 1998, pp. 301–307.
5. J. Holtz and U. Boelkens, “Direct frequency convertor with sinusoidal line currents for speed-variable AC motors,” IEEE Trans. Ind. Electron., vol. 36, no. 4, pp. 475–479, Nov. 1989.
6. L. Huber and D. Borojevic, “Space vector modulated three-phase to three-phase matrix converter with input power factor correction,” IEEE Trans. Ind. Appl., vol. 31, no. 6, pp. 1234–1246, Nov. 1995.
7. P. Wheeler, J. Rodriguez, J. Clare, L. Empringham, and A. Weinstein, “Matrix converters: A technology review,” IEEE Trans. Ind. Electron., vol. 49, no. 2, pp. 276–288, Apr. 2002.
8. P. Zwimpfer and H. Stemmler, “Modulation and realization of a novel two-stage

matrix converter," in Proc. Brazilian Power Electron. Conf., 2001, pp. 485–490.
9. L. Wei and T. A. Lipo, "A novel matrix converter topology with simple commutation," in Proc. IEEE Ind. Appl. Soc. Annu. Meeting, 2001, pp 1749–1754.
10. L. Wei and T. A. Lipo, "Matrix converter with reduced number of switches," in Proc. Record 20th W'EMPEC Anniversary Meeting, Oct. 2001, pp. 580–586.
11. J. W. Kolar, F. Schafmeister, S. D. Round, and H. Ertl, "Novel three-phase ac-ac sparse matrix converters," IEEE Trans. Power Electron., vol. 22, no. 5, pp. 1649–1661, Sep. 2007.
12. R. Cardenas, R. Pena, P. Wheeler, J. Clare, and G. Asher, "Control of the reactive power supplied by a WECS based on an induction generator fed by a matrix converter," IEEE Trans. Ind. Electron., vol. 56, no. 2, 429–438, Feb. 2009.
13. J. Monteiro, J. Silva, S. Pinto, and J. Palma, "Matrix converter-based unified power-flow controllers: Advanced direct power control method," IEEE Trans. Power Del., vol. 26, no. 1, pp. 420–430, Jan. 2011.
14. F. Schafmeister and J. W. Kolar, "Novel hybrid modulation schemes significantly extending the reactive power control range of all matrix converter topologies with low computational effort," IEEE Trans. Ind. Electron., vol. 52, no. 1, pp. 194–210, Jan. 2012.
15. M. Rivera, J. Rodriguez, J. Espinoza, T. Friedli, J. Kolar, A. Wilson, and C. Rojas, "Imposed sinusoidal source and load currents for an indirect matrix converter," IEEE Trans. Ind. Electron., vol. 59, no. 9, pp. 3427– 3435, Sep. 2012.
16. S. Yao, S. Mei, W. Hui, and G. Wei-hua, "Nonlinearity analysis and compensation strategies for two-stage matrix converter," in Proc. CSEE, Apr. 2010, pp. 20–27.
17. H. Akagi, A. Nabae, and S. Atoh, "Control strategy of active power filters using multiple voltage source PWM converters," IEEE Trans. Ind. Appl., vol. IA-22, no. 3, pp. 460–465, May 1986.
18. D. Pedder, A. Brown, J. Ross, and A. Williams, "A parallel-connected active filter for the reduction of supply current distortion," IEEE Trans. Ind. Electron., vol. 47, no. 5, pp. 1108–1117, Oct. 2000.
19. M. Jantsch and C. W. G. Verhoeve, "Inverters with three-phase output and without electrolyte capacitor for improved lifetime, efficiency and costs of grid connected systems," presented at the 14th Eur. Photovoltaic Solar Energy Conf., Barcelona, Spain, Jun. 1997.
20. H. Yoo and S. Sul, "A new circuit design and control to reduce input harmonic current for a three-phase ac machine drive system having a very small dc-link capacitor," in Proc. 25th Annu. IEEE Appl. Power Electron. Conf. Expo., Feb. 2010, pp. 611–618.
21. T. Soeiro, T. Friedli, and J. W. Kolar, "Three-phase high power factor mains interface concepts for electric vehicle battery charging systems," in Proc. 27th Annu. IEEE Appl. Power Electron. Conf. Expo., Feb. 2012, pp. 2603–2610.
22. S. Kim, P. N. Enjeti, D. Rendusara, and L. J. Pitel, "A new method to improve THD and reduce harmonics generated by a three phase diode rectifier type utility interface," in Proc. IEEE Ind. Appl. Soc. Annu. Meet-ing, 1995, pp. 1071–1077.
23. P. Pejovic,´ "Low harmonic three phase rectifier," in Power Electron. Spec. Conf., Jun. 2000, pp. 1029–1034.
24. N. Vazquez, H. Rodriguez, C. Hernandez, E. Rodriguez, and J. Arau, "Three-phase rectifier with active current injection and high efficiency," IEEE Trans. Ind. Electron., vol. 56, no. 1, pp. 110–119, Jan. 2009.
25. M. Jankovic, M. Darijevic, P. Pejovic, J. Kolar, and Y. Nishida, "Hybrid three-phase

rectifier with switched current injection device," in Proc. 15th Int. Power Electron. Motion Control Conf., 2012, pp. LS3e.2-1–LS3e.2-7.
26. J. Kolar and T. Friedli, "The essence of three-phase PFC rectifier systems," in Proc. 3rd IEEE Int. Telecommun. Energy Conf., 2011, pp. 1–27.
27. T. Soeiro, F. Vancu, and J. W. Kolar, "Hybrid active 3rd harmonic cur-rent injection mains interface concept for DC distribution systems," IEEE Trans. Power Electron., vol. 28, no. 1, pp. 7–13, Jan. 2013.
28. T. Nussbaumer, M. Heldwein, and J. Kolar, "Differential mode input filter design for a three-phase buck-type PWM rectifier based on modeling of the EMC test receiver," IEEE Trans. Ind. Electron., vol. 53, no. 5, pp. 1649–1661, Oct. 2006.
29. D. G. Holmes and T. A. Lipo, Pulse Width Modulation for Power Convert-ers: Principles and Practice. Piscataway, NJ, USA: IEEE Press, 2003.
30. Klumpner and F. Blaabjerg, "Modulation method for a multiple drive system based on a two-stage direct power conversion topology with re-duced input current ripple," IEEE Trans. Power Electron., vol. 20, no. 4, pp. 922–929, Jul. 2005.
31. Wang and G. Venkataramanan, "Analytical modeling of semiconduc-tor losses in matrix converters," in Proc. IEEE Power Electron. Motion Control Conf., 2006, pp. 1–8.